In Silico and In Vitro Filters for the Fast Estimation of Skin Permeation and Distribution of New Chemical Entities

Giorgio Ottaviani, Sophie Martel, and Pierre-Alain Carrupt*

LCT-Pharmacochimie, Section des sciences pharmaceutiques, Université de Genève, Université de Lausanne, Quai Ernest-Ansermet 30, CH-1211, Genève 4, Suisse

Received September 25, 2006

The development of in silico and in vitro tools to estimate or predict the passive human skin permeation and distribution of new chemical entities, useful in dermal drug delivery, in absorption studies of toxic compounds, and in the cosmetics industry, is presented. In vitro permeation parameters were measured using the artificial membrane PAMPA-skin. The Volsurf approach was then applied to extract pertinent descriptors from molecular interaction fields characterizing the molecular structure of tested compounds. Two useful three-dimensional solvatochromic models able to predict PAMPA permeation parameters directly from the molecular structure were obtained using the partial least squares analysis. The models also provide valuable information to understand the link between physicochemical and structural properties of tested compounds and their interactions with the artificial membrane PAMPA-skin and can be useful to rapidly estimate their permeation through the human skin.

Introduction

The development of a new artificial membrane (PAMPA[a]-skin) for the fast determination of passive human skin permeation has recently been presented.[1] The good correlation obtained between permeability coefficients determined through human skin (log K_p) and those determined through PAMPA-skin (log P_e) and (for a limited set of compounds) between stratum corneum (SC)/water partition coefficient (log P_{sc}) values and the PAMPA-skin membrane retention proved that the artificial membrane can mimic the main barrier properties of SC.

The transport of permeants through this artificial membrane in terms of structure−permeability relationships was investigated in this work. Indeed QSAR models will better identify the most important physicochemical and structural properties of tested compounds affecting their interactions with PAMPA-skin and thus also offer fast estimations of their behavior on human skin. Accordingly, the development of three-dimensional (3D) solvatochromic models for the permeation of compounds through the artificial membrane PAMPA-skin are presented in this work using an extended set of 69 compounds. The solvatochromic descriptors were extracted from five molecular interaction fields (MIFs) using the Volsurf[2] approach and then correlated to the experimental parameters determined with PAMPA-skin.

Predicting Skin Permeability. The assessment of a global predictive model requires, besides consistent and reliable data, that the process to be modeled occurs with the same mechanism for all tested compounds. It is well-known that the major determinant of percutaneous transport rate, especially for hydrophobic molecules, is the passive diffusion through the lipid matrix between the corneocytes.[3] Interestingly it was recently found that passive diffusion mechanisms may also control the permeation of relatively hydrophilic solutes ($-1 < \log P_{oct} < 0$).[4] Furthermore, the limited experimental permeation data for polar compounds do not allow a systematic research focusing upon the commonly referred porous/polar pathway.[5,6] In effect, most of the permeation data that have been analyzed derive from the Flynn database[7] and include a very limited number of polar solutes.

As shown above, it is reasonable to believe that the passive diffusion pathway through the SC controls the permeation of most compounds whose permeation through human skin has been experimentally determined.

Many quantitative structure−permeation relationship (QSPeR) models have been developed by researchers to model passive percutaneous penetration of exogenous chemicals.[8,9] The most popular predictive model is the equation proposed by Potts and Guy,[3] derived from the octanol−water partition coefficient (P_{oct}) and the molecular weight to describe the penetration of compounds through the skin. Different approaches based on electrotopological and steric descriptors[8,10] and other theoretical descriptors[11] are reported in the literature.

Solvatochromic analyses (linear solvation energy relationships (LSERs)) have also been widely used in correlations with biological, chemical, and physical properties involving solute−solvent interactions for a large number of chemicals.[12] The general form of the LSER equation includes as independent variables a cavity/bulk term, a polarizability term, and a hydrogen bond term(s). Abraham and Martins[13] recently proposed a fairly good permeation model for 119 solutes based on the general linear free-energy relationship (LFER)

$$\log K_p = c + eE + sS + aA + bB + vV \qquad (1)$$

where K_p is the human skin permeability coefficient, E is the solute excess molar refractivity, S is the dipolarity/polarizability, A and B are the hydrogen-bond acceptor and donor activity, respectively, and V is the molecular volume. Although predictive models have been developed, the use of two-dimensional descriptors both in QSPeRs and in LSER analysis do not take into account the 3D aspects of molecular structures, thus limiting the development of more realistic models especially for flexible molecules.

* To whom correspondence should be addressed. Tel.: +41 22 379 3359. Fax: +41 22 379 3360. E-mail: pierre-alain.carrupt@pharm.unige.ch.

[a] Abbreviations: PAMPA, parallel artificial membrane permeability assay; MIFs, molecular interaction fields; PLS, partial least squares; log K_p, logarithm of permeability coefficient measured in vitro through human skin; log P_e, logarithm of effective permeability coefficient measured with PAMPA technique; log P_{sc}, logarithm of the stratum corneum/water partition coefficient; QSPeRs, quantitative structure permeation relationships; LSER, linear solvation energy relationship; LFER, linear free-energy relationship; MLP_{ho}, hydrophobic contribution of molecular lipophilicity potential; MHBPs, acceptor and donor molecular hydrogen-bonding potentials; DMSO, dimethyl sulfoxide; IPM, isopropyl myristate; τ_{LAG}, lag time of diffusion; LV, latent variable; SC, stratum corneum.

10.1021/jm0611105 CCC: $37.00
Published on Web 01/19/2007

The calculation of molecular properties from 3D MIFs has generated a novel approach to correlate 3D molecular structures with pharmacokinetic and physicochemical properties.[2] Recently, a partial least squares (PLS) analysis based on 3D molecular descriptors calculated with Volsurf procedure was reported to study skin permeation of naproxen derivatives.[14] Although this study offers a valuable tool to derive significant, internally predictive quantitative models for structure−permeation relationships, the interpretation in terms of intermolecular interactions was limited due to the congeneric nature of the series explored.

In the present study, two 3D solvatochromic models were developed for the prediction of compound permeation and distribution through PAMPA-skin membrane using molecular descriptors calculated with Volsurf from five MIFs: the hydrophobic part of the molecular lipophilicity potential (ML-P_{ho}),[15] the acceptor and donor molecular hydrogen-bonding potential (MHBPs),[16] and the GRID "DRY" and "H_2O" fields.[17]

Results and Discussion

Classification of Permeants. In PAMPA-skin, compounds were grouped according to experimental values of membrane retention (%*R*) and the permeation parameter (%$C_A(t)/C_D(0)$). It was shown that compounds highly permeable through human skin (($\log K_p \geq -6$) can be differentiated by PAMPA-skin into two groups, namely, compounds trapped in the artificial membrane and compounds not retained within the membrane, while compounds with low permeability ($\log K_p < -6$) present no membrane retention and low $C_A(t)/C_D(0)$ values.[1]

As a consequence, three classes of compounds were formed in accordance with their experimental values of *R* and $C_A(t)/C_D(0)$. Accordingly, compounds with $C_A(t)/C_D(0) < 20\%$ and negligible %*R* were assigned to class (I), compounds with $C_A(t)/C_D(0) > 20\%$ and $R < 23\%$ to class (II) and compounds with $R > 23\%$ to class (III).

Permeation through PAMPA-Skin for the Additional Dataset. To develop a comprehensive model, a set of 38 compounds in addition to the set (31 compounds) previously published[1] was selected for permeation measurements through PAMPA-skin artificial membrane. Additional compounds were selected according to their chemical diversity and available human skin permeability coefficient values ($\log K_p$). Permeation experiments were thus carried out for these compounds on PAMPA-skin using the protocol previously described (see Table 1 for experimental results). Figure 1 shows the relationship between membrane retention *R* and the permeation parameter $C_A(t)/C_D(0)$ for the 38 tested compounds together with the previous 31 compounds with a color scheme representing the three classes described above. For compounds belonging to classes II and III, there is a negative correlation between membrane retention (*R*) and permeation ($C_A(t)/C_D(0)$), meaning that for these compounds, the membrane behaves like a trap.

Eight compounds (atenolol, dibucaine, diethylaniline imipramine, sulfacarbamide, sulfacetamide sulfanilamide, and trifluoroperazine) did not permeate the membrane after a 7 h incubation time (%$C_A(t)/C_D(0) < 1$) and, therefore, it was not possible to determine the effective permeability coefficient ($\log P_e$) for these chemicals.

Permeability coefficients determined through PAMPA-skin ($\log P_e$) were then plotted against the available permeability coefficient values determined through human skin: the good correlations obtained between $\log P_e$ and $\log K_p$ for the extended set confirm the efficacy of the artificial membrane PAMPA-skin for the fast prediction of compounds' permeation through human skin (Figure 2).

Permeation Described by $\log P_{oct}$ and Molecular Weight. The most popular predictive model of skin permeation is the equation proposed by Potts and Guy[3] derived from the octanol−water partition coefficient (P_{oct}) and molecular weight (MW). Multiple regression analysis for human skin permeability coefficient values ($\log K_p$) and for effective permeability coefficients ($\log P_e$) determined through PAMPA-skin were done for tested compounds based on the descriptors proposed by Potts and Guy. The analysis of the coefficients in eqs 2 and 3 shows that the permeation of solutes through human skin and through PAMPA-skin are similarly influenced by MW and $\log P_{oct}$, although the latter seems to have more importance in the description of $\log K_p$. So, the permeation of a molecule through PAMPA-skin membrane, in analogy to SC permeation, increases as its lipophilicity increases, while as the molecule becomes bigger, its diffusion through the membrane is reduced.

$$\log K_p = 0.77 \log P_{oct} - 0.0073\mathrm{MW} - 5.98$$
$$n = 38;\ r^2 = 0.81;\ s = 0.42;\ q^2 = 0.77 \quad (2)$$

$$\log P_e = 0.47 \log P_{oct} - 0.0050\mathrm{MW} - 4.58$$
$$n = 38;\ r^2 = 0.73;\ s = 0.33;\ q^2 = 0.67 \quad (3)$$

A multiple regression analysis was then performed for $\log P_e$ using the extended data set. The total set of 69 compounds was reduced to 61 compounds because no $\log P_e$ was measured for eight compounds (see above). A first investigation of the predictive residual plot revealed that spironolactone was not well predicted. After the removal of this outlier, the model demonstrated a good predictivity ($q^2 = 0.72$) and confirmed that $\log P_{oct}$ and MW are pertinent descriptors to predict the permeation of compounds through PAMPA-skin artificial membranes

$$\log P_e = 0.45 \log P_{oct} - 0.0052\mathrm{MW} - 4.50$$
$$n = 60;\ r^2 = 0.75;\ s = 0.33;\ q^2 = 0.72 \quad (4)$$

3D Solvatochromic Model for the Quantitative Determination of $\log P_e$. Although $\log P_{oct}$ and MW are successful descriptors of some permeation processes, it might be advantageous to describe the transport of permeants through the membranes in terms of their pure physicochemical properties. In particular, partitioning coefficients in the *n*-octanol/water biphasic system do not fully express the capacity of solutes to perform hydrophilic interactions with the skin. Indeed the balance between hydrophilic interactions revealed by the $\log P_{oct}$ may largely differ from the balance of interactions with the intercellular components of skin as already demonstrated for partition coefficients measured in other biphasic systems.[18−20] A multiple regression analysis relating human skin permeability coefficients to physicochemical parameters independent of organic-phase partition coefficients has been reported using a set of 37 compounds consisting mainly of phenol derivatives and alkyl alcohols.[20] The study demonstrated that the transport of permeants across the SC was mainly controlled by the molecular size and water hydrogen bond activity.

A PLS model was then developed for the 61 compounds using the effective permeability coefficient ($\log P_e$) values as dependent variable (Y) and 3D solvatochromic descriptors as matrix X. I-MLP_{ho}, I-DRY, S, and G molecular descriptors being poorly related with $\log P_e$ were eliminated in the study. The predictive ability of the models was assessed using the "leave-one-out" cross validation procedure.

The inspection of the predictive residual plots showed four compounds not well predicted (outliers): antipyrine, caffeine, sulfabenzamide, and sulfadiazine. For sulfabenzamide and

Table 1. MW, Lipophilicity Values in Octanol−Water System, log P_{oct}, Permeability Coefficients Obtained through Human Skin (log K_p), Membrane Retention (R), $C_A(t)/C_D(0)$, and Effective Permeability Coefficient (log P_e) Values Obtained after a 7 h Incubation Time Using the PAMPA-skin membrane (70% Silicone−30% IPM)[a]

cmpd	MW	log P_{oct}[b]	log K_p[27]	R (%)	$C_A(t)/C_D(0)$(%)	log P_e
			Original Set			
2-amino-4-nitrophenol	154.1	1.18[c]	−6.62	<1	18.2 ± 0.8	−4.84 ± 0.05
2-naphthol	144.2	2.70	−5.11	20.1 ± 1.1	36.5 ± 0.7	−4.19 ± 0.03
2-nitro-*p*-phenylendiamine	153.1	0.53[d]	−6.86	<1	17.4 ± 0.5	−4.94 ± 0.02
4-bromophenol	173.0	2.59	−5.00	10.9 ± 0.9	44.1 ± 0.8	−3.90 ± 0.08
4-chlorophenol	128.6	2.39	−5.00	16.8 ± 0.5	39.4 ± 0.8	−4.10 ± 0.06
4-ethylphenol	122.2	2.47	−5.01	13.6 ± 2.3	41.6 ± 1.7	−4.05 ± 0.08
4-nitrophenol	139.1	1.91	−5.81	4.6 ± 2.6	39.9 ± 0.9	−4.32 ± 0.06
atrazine	215.7	2.61	−5.56	13.5 ± 4.8	38.8 ± 0.6	−4.21 ± 0.05
benzyl nicotinate	213.2	2.40	−5.35	40.6 ± 1.6	26.0 ± 1.0	−4.26 ± 0.02
caffeine	194.2	−0.07	−7.56[28]	<1	4.3 ± 0.2	−5.63 ± 0.02
antipyrine	188.2	0.38	−7.74	<1	1.2 ± 0.5	−6.20 ± 0.17
corticosterone	346.5	1.94	−7.08[28]	<1	13.6 ± 0.1	−5.06 ± 0.01
dexamethasone	392.5	2.01	−7.75[28]	<1	3.2 ± 0.4	−5.75 ± 0.05
diclofenac	296.2	4.51[e]	−5.30	4.0	11.0 ± 1.9	−4.33 ± 0.11
ephedrine	165.2	0.93	−5.75	<1	21.8 ± 4.3	−4.81 ± 0.12
hydrocortisone	362.5	1.61	−7.19[29]	<1	2.2 ± 0.4	−5.94 ± 0.07
indomethacin	257.8	4.27	−5.39	52.8 ± 5.3	21.3 ± 2.7	−4.20 ± 0.08
isoquinolina	129.2	2.08	−5.33	7.3 ± 4.1	44.5 ± 1.5	−4.05 ± 0.04
ketoprofen	254.3	3.12	−4.70	12.1 ± 1.9	38.5 ± 0.8	−4.25 ± 0.01
lidocaine	234.3	2.26	−5.32[30]	9.7 ± 3.3	36.8 ± 1.0	−4.35 ± 0.03
methyl nicotinate	137.1	0.87	−6.04	10.7 ± 0.4	37.2 ± 1.0	−4.32 ± 0.06
naproxene	230.3	3.34	−4.97	23.1 ± 3.3	36.2 ± 1.2	−4.11 ± 0.11
nicotine	162.2	1.17	−5.26	4.1 ± 1.1	30.2 ± 4.9	−4.58 ± 0.12
phenobarbital	232.2	1.47	−6.90	<1	11.7 ± 0.4	−5.15 ± 0.02
phenol	94.1	1.46	−5.64	<1	46.7 ± 0.6	−4.14 ± 0.03
piroxicam	331.3	3.06	−6.02	7.2 ± 0.9	37.7 ± 0.6	−4.35 ± 0.02
progesterone	314.5	3.87	−5.08[29]	73.5 ± 2.0	8.6 ± 0.6	−4.56 ± 0.06
resorcinol	110.1	0.80	−7.18	<1	4.4 ± 0.8	−5.62 ± 0.08
salycilic acid	138.1	2.26	−5.45	5.7 ± 1.2	43.1 ± 1.6	−4.16 ± 0.02
testosterone	288.4	3.32	−5.83[31]	9.2 ± 1.6	42.9 ± 1.0	−4.11 ± 0.04
thymol	150.2	3.30	−4.83	66.2 ± 3.7	13.9 ± 2.1	−4.34 ± 0.06
			Extended Set			
1-chloro−2-nitrobenzene	157.6	2.24		45.7 ± 5.9	24.2 ± 1.8	4.05 ± 0.07
2,4,6-tricholorophenol	197.4	3.69	−4.78	75.0 ± 4.8	10.3 ± 3.2	−4.33 ± 0.15
2-amino-naphtalene	143.2	2.28		18.2 ± 2.4	36.4 ± 2.6	−4.23 ± 0.10
3,4-xylenol	122.2	2.23	−5	11.1 ± 6.0	41.2 ± 3.5	−4.16 ± 0.05
4-phenylbutyric acid	164.2	2.42		11.3 ± 2.9	42.6 ± 2.6	3.87 ± 0.11
5-phenylvaleric acid	178.3	2.85[f]		19.6 ± 2.3	38.0 ± 1.9	−4.10 ± 0.10
acridine	179.2	3.40		56.5 ± 2.1	17.4 ± 1.2	−4.37 ± 0.0
atenolol	266.4	0.22[e]		<1	<1	
benzidine	184.3	1.34		3.8 ± 2.3	35.0 ± 0.6	−4.46 ± 0.0
benzoic acid	122.1	1.87	−5.08	<1	44.7 ± 2.9	−4.21 ± 0.12
betamethasone	392.5	2.01	−7.17	<1	2.8 ± 0.7	−5.84 ± 0.14
butyl-*p*-aminobenzoic acid	193.2	2.87	−5.14	39.4 ± 0.6	25.7 ± 1.0	−4.30 ± 0.05
diazepam	284.8	2.92[f]		24.6 ± 3.6	33.1 ± 1.5	−4.26 ± 0.02
dibucaine	343.5	4.40		82.8 ± 7.9	<1	
dienestrol	266.4	4.50[c]		78.1 ± 0.1	11.4 ± 2.0	−4.53 ± 0.35
diethylaniline	149.3	3.31		84.3 ± 9.6	<1	
ethyl-*p*-aminobenzoic acid	165.2	1.86	−5.27	2.9 ± 0.4	42.6 ± 1.0	−4.25 ± 0.03
flurbiprofen	244.3	3.99[e]		67.6 ± 1.2	14.6 ± 0.6	−4.21 ± 0.0
imipramine	280.4	4.39[e]		69.1 ± 11.0	<1	
o-cresol	108.1	1.94	−5.36	6.8 ± 1.8	43.4 ± 1.5	−4.18 ± 0.03
oxazepam	286.7	2.24		<1	22.0 ± 1.0	−4.64 ± 0.03
perphenazine	404.0	4.2		25.2 ± 4.6	24.3 ± 2.7	−4.56 ± 0.0
phenylacetic acid	136.2	1.41		<1	33.2 ± 0.7	−4.54 ± 0.0
phenylheptanoic acid	206.3	3.63		41.6 ± 7.8	22.0 ± 4.8	−4.25 ± 0.12
prednisone	358.5	1.46		<1	1.7 ± 0.3	−6.04 ± 0.10
propranolol	259.4	3.48[e]		17.7 ± 1.8	36.1 ± 2.5	−4.25 ± 0.08
pyridine	79.1	0.65		12.3 ± 6.5	35.6 ± 3.7	−4.35 ± 0.06
spirolactone	416.6	2.26		20.9 ± 6.6	32.7 ± 4.3	−4.33 ± 0.07
sulfabenzamide	276.3	1.46[f]		<1	4.1 ± 0.6	−5.65 ± 0.07
sulfacarbamide	229.3	−1.1		<1	<1	
sulfacetamide	214.3	−0.96		<1	<1	
sulfadiazine	250.3	−0.12[e]		<1	1.2 ± 0.4	−6.20 ± 0.14
sulfadimethoxine	310.4	1.63		<1	6.6 ± 0.3	−5.25 ± 0.02
sulfanilamide	172.2	−0.62		<1	<1	
tolbutamide	270.4	2.34		<1	42.3 ± 4.6	−4.29 ± 0.15
triamcinolone	394.5	1.16		<1	1.2 ± 0.5	−6.24 ± 0.21
trifluoroperazine	407.5	5.03		78.2 ± 7.0	<1	
warfarine	308.4	3.54[e]		14.9 ± 5.4	37.8 ± 2.8	−4.24 ± 0.02

[a] Permeability coefficients (K_p, P_e) are expressed in [cm/s]. [b] From ref 32. [c] Values calculated using CLOGP version 4.91 (Daylight Chemical Information System, Inc., Irvine, CA, 2005). [d] From ref 33. [e] From ref 24. [f] From A. Galland, 2003, personal communication.

sulfadiazine, a poor parametrization of the sulfamide group is suspected. Finally, for antipyrine and caffeine, further investigations are in progress to better understand their poor predictions.

After the removal of the outliers, the PLS statistical interpretation for the solvatochromic model led to a two-component model, which explained 80% of the total variance of the Y matrix. The plot of experimental versus predicted log P_e values is shown in Figure 3. The predictivity of the model ($q^2 = 0.74$) is comparable to that obtained using log P_{oct} and MW descriptors ($q^2 = 0.72$, eq 4), suggesting that the 3D solvatochromic model provides a good quantitative determination of PAMPA-skin permeability coefficients.

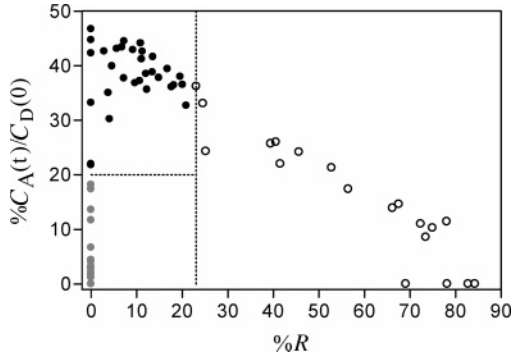

Figure 1. Membrane retention (%R) and amount of compounds found in the acceptor compartment after 7 h incubation time (%$C_A(t)/C_D(0)$) using 70% silicone−30% IPM membrane. Compounds are colored according to membrane retention (R) and the permeation parameter ($C_A(t)/C_D(0)$ values (see text for details), namely, low permeants (gray circles, class I), high permeants (dark circles, class II), and permeants with high membrane retention (open circles, class III).

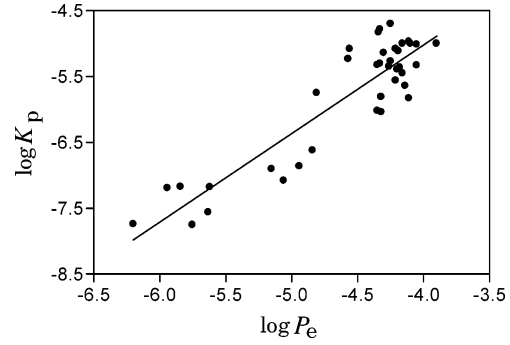

Figure 2. Correlation between effective permeability coefficients log P_e determined through 70% silicone−30% IPM membrane and human skin permeability coefficient log K_p for the extended set. The line was obtained by the following linear regression equation: log K_p = 1.34 (± 0.11) log P_e + 0.36 (± 0.49); (n = 38; r^2 = 0.82; s = 0.4; F = 158).

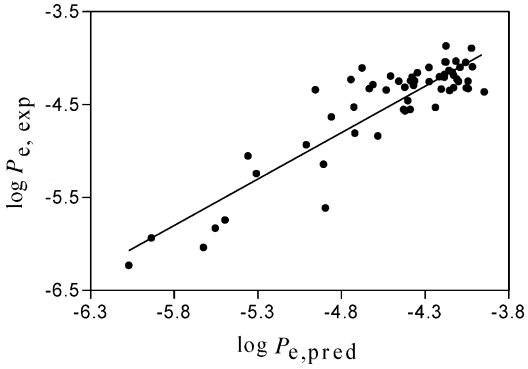

Figure 3. Plot of predicted vs experimental effective permeability coefficient (log P_e) using the PLS 3D solvatochromic model (r^2 = 0.80, q^2 = 0.74, n = 57).

Figure 4 shows the PLS coefficient plot of the model for the first two latent variables (LVs). The molecular descriptors positively correlated with the log P_e are those related to dipolarity/dipolarisability (V-DRY), hydrophobicity (V-MLP$_{ho}$), and localized hydrophilic regions (I-MHBP$_{ac}$, I-MHBP$_{do}$), while those negatively affecting the permeation through the membrane are those describing hydrophilic interactions (V-MHBP$_{ac}$, V-MHBP$_{do}$) and molecular volume and shape (V, R). So, according to the model, the permeability through PAMPA-skin membrane is bigger for small and hydrophobic molecules presenting localized hydrophilic regions.

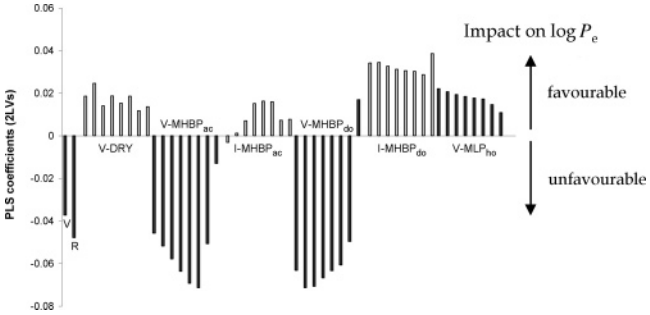

Figure 4. PLS coefficient plot for the two LVs calculated with the 3D solvatochromic model for the prediction of log P_e.

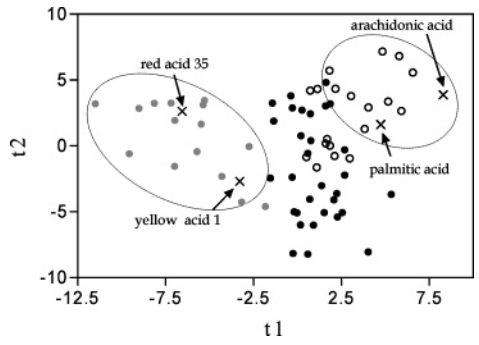

Figure 5. Discriminant analysis PLS score plot. Palmitic acid, arachidonic acid, red acid 35, and yellow acid 1 are represented with crosses (X). See Figure 1 for other color codes.

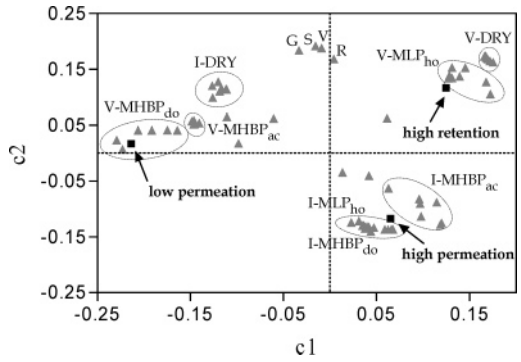

Figure 6. Discriminant analysis PLS loading plot of the extended set. Molecular descriptors are represented as gray triangles and dependent variables (Y) as black squares.

Discriminant-Analysis PLS Model. A discriminant PLS solvatochromic model using experimental values of membrane retention (%R) and permeation parameter %$C_A(t)/C_D(0)$ was then developed for the total set of 65 compounds (after the removal of the four outliers: antipyrine, caffeine, sulfabenzamide, and sulfadiazine) using 68 descriptors extracted with Volsurf from the MIFs previously described (X data matrix). The three classes representing the experimental values of %R and %$C_A(t)/C_D(0)$ were organized in a Y matrix, the DA-PLS analysis gave a two-component model. Figure 5 shows the score plot obtained from the first two LVs. The first LV discriminates compounds with poor permeation and negligible membrane retention (class I) from the others (classes II and III), while the second LV separates relatively well compounds from class II and compounds from class III.

Figure 6 shows the loading plot of the first LV versus the second LV. It is important to recall that this plot represents the original variables in the space of the LVs. If the angle formed by two variables in the plot respect to the interception of axis is small it means that they contain similar information, for

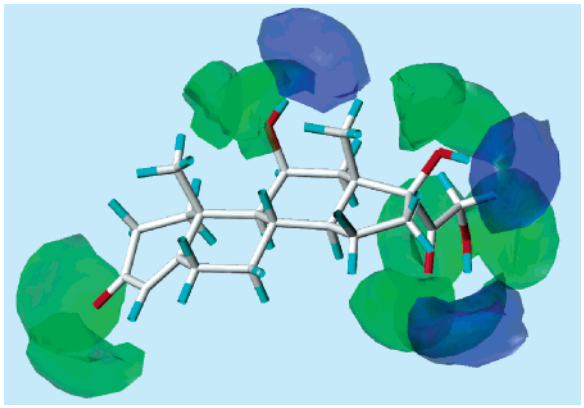

Figure 7. MHBP molecular fields of hydrocortisone calculated at 0.05 potential level. Volumes of acceptor H-bonds (V-MHBP$_{ac}$) and donor H-bonds (V-MHBP$_{do}$) regions are represented, respectively, in green and in blue.

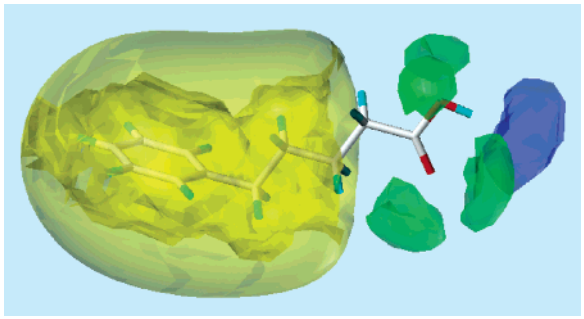

Figure 8. MHBP and MLP$_{ho}$ molecular fields of 5-phenylvaleric acid calculated respectively at 0.05 and at 0.5 potential level. Volume of acceptor H-bonds (V-MHBP$_{ac}$) is represented in green, volume of donor H-bonds (V-MHBP$_{do}$) is represented in blue, and the volume of hydrophobic regions (V-MLP$_{ho}$) is represented in yellow.

example, an angle of 90° denotes that the variables are independent of each other, while an angle of 180° indicates that variables are inversely correlated to each other. The compounds characterized by low permeation through the artificial membrane (class I) are mainly influenced by polar descriptors (V-MHBP$_{ac}$, V-MHBP$_{do}$). For example, Figure 7 illustrates the volumes of H-bond acceptor and donor regions (V-MHBP$_{ac}$, V-MHBP$_{do}$) calculated at 0.05 potential level for the low permeant hydrocortisone. As a result, the presence of H-bonding donor acid groups and H-bonding acceptor basic groups in the compounds decreases their permeation through the artificial membrane. An inverse relationship was also found between hydrogen bond activity and skin permeability,[13,20] suggesting that hydrophilic chemicals diffuse slowly through the SC.

Conversely, high permeants through PAMPA-skin membrane (class II) are mostly correlated with hydrophobic (I-MLP$_{ho}$), donor-hydrophilic (I-MHBP$_{do}$), and acceptor-hydrophilic (I-MHBP$_{ac}$) integy moment descriptors. Moreover, the second LV in the loading plot shows that these compounds are also characterized by low molecular size and shape descriptors (R, V, S, G). Integy moments express the unbalance between the center of mass of a molecule and the barycentre of hydrophobic or hydrophilic regions around it. When the integy moment is high, there is a clear concentration of hydrophobic or hydrated regions in only one part of the molecule. Therefore, molecules that highly permeate the membrane present localized hydrophobic and hydrophilic regions. Figure 8 shows the MHBP and MLP$_{ho}$ molecular fields of 5-phenylvaleric acid, a molecule that easily permeates the artificial membrane. Acceptor H-bonds (V-MHBP$_{ac}$) and H-bond (V-MHBP$_{do}$) volumes calculated at the

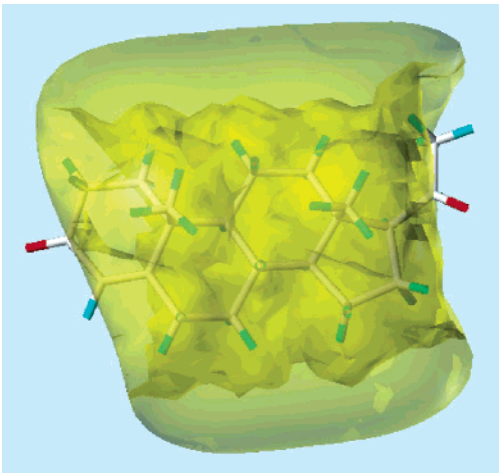

Figure 9. MLP$_{ho}$ molecular fields of progesterone calculated at 0.5 potential level. The volume of hydrophobic regions (V-MLP$_{ho}$) is represented in yellow.

0.05 potential level are represented, respectively, in green and blue, while the volume of hydrophobic region (V-MLP$_{ho}$), calculated at the 0.5 potential level, is represented in yellow. The presence of localized hydrophobic and hydrophilic regions is clearly represented by those molecular fields. Thus, although the presence of polar groups negatively affects the overall permeation through the membrane, the asymmetric distribution of these moieties provides a positive contribution to the permeability. The presence of isopropyl myristate (IPM) in the artificial membrane presenting a localized hydrophilic (basic) moiety could explain the high permeation of compounds presenting asymmetric distribution of polar regions. Because the lipids constituting the SC present localized hydrophilic and hydrophobic regions as well, it could be reasonable to conclude that the presence of localized hydrophobic and donor groups may enhance the permeation of compounds through the SC.

The descriptors associated to the class III (high membrane retention) in the loading plot (Figure 6) are those related to dipolarity/dipolarizability (V-DRY) and hydrophobicity (V-MLP). The presence of nondirectional electrostatic interactions and hydrophobic interactions between permeants and the artificial membrane constituents, thus, positively contribute to membrane retention. The MLP$_{ho}$ molecular fields of progesterone calculated at 0.5 potential level are shown in Figure 9. Progesterone is a molecule with a high membrane retention (R = 73.5%), and the existence of a large hydrophobic region is well shown by the MLP$_{ho}$ isopotential surface. The positive contribution of hydrophobicity to skin permeation has been shown in many predictive models,[8,9] while the effect of dipolarity/dipolarizability has not been studied in detail and has not revealed particular influence on skin permeation.[13]

Use of Discriminant In Silico PAMPA-Skin Filter. The in silico PAMPA-skin filter allows to predict relatively well which class (based on membrane retention (R) and permeation parameter $C_A(t)/C_D(0)$) a new compound belongs by the simple determination of its 3D solvatochromic descriptors. This information could guide the selection of new compounds to be tested through the PAMPA-skin artificial membrane. Reservoir properties of SC have been demonstrated to exist,[21] and, thus, the investigation of these functions is essential in dermatologic and cosmetic studies.[22] For example, dermatological and cosmetic applications require compounds to be absorbed and to remain at a certain extent in skin layers. The membrane retention of compounds determined in PAMPA-skin artificial membrane seems to reflect the affinity of compounds with SC[1]

and, as a consequence, their potential to get trapped in it. Thus, the prediction of a high membrane retention (class III) for a compound could provide interesting hints regarding the capacity of that chemical to get accumulated in the SC, and therefore, later it would be interesting to determine experimentally the membrane retention of that compound in PAMPA-skin. Moreover, it has been demonstrated that compounds belonging to classes II (high permeation) and III (high membrane retention) are characterized by high permeation through the human skin ($\log K_p > -6$), while compounds from class I do not permeate the skin very well ($\log K_p < -6$). So the use of in silico PAMPA-skin filter may allow an estimation of the potential penetration through human skin of an unknown chemical. It would be interesting to enlarge the data set to further assess the predictive capability of the model.

An application based on the discriminant in silico model is presented below. Two chemicals used in hair dyes (yellow acid 1 and red acid 35) and two emollient agents used in cosmetics (palmitic acid and arachidonic acid) were selected and their molecular descriptors were calculated with the procedure reported above. The projection of the selected compounds in the model are shown in Figure 5. Yellow acid 1 and red acid 35 are predicted as low permeants by the discriminant model, while palmitic acid and arachidonic acid are predicted with high membrane retention (i.e., high affinity for SC). These results are in agreement with qualitative experimental data (hair dyes must preferably not penetrate the skin,[23] while emollient agents are normally trapped in the SC), and confirm the good predictability of the model.

Conclusions

The in silico and in vitro filters presented are the building blocks of an *in combo* approach for a better prediction of skin permeation and distribution of new chemical entities. In this study, two 3D solvatochromic models were developed for the prediction of compound permeation and distribution from PAMPA-skin permeation experiments. The quantitative structure-PAMPA-permeation model for log P_e provides clear information of the permeant structural properties responsible for the permeation through the artificial membrane and could also be used to estimate the permeability coefficients through human skin (K_p). The discriminant-PLS model differentiating compounds according to their experimental values of membrane retention and permeation can be used as a fast in silico filter that can guide the selection and the design of compounds to be tested in permeation experiments and permit a rapid estimation of the penetration and distribution of compounds through human skin.

Experimental Section

Chemicals. All compounds were purchased from Sigma (division of Fluka Chemie AG, Buchs, Switzerland). DMSO (purity grade >99.7%) was purchased from Acros Organics (Chemie Brunschwig AG, Basel, Switzerland). IPM (purity grade >95%), silicone oil (DC 200), and hexane (purity grade >99.5%) were purchased from Fluka. The buffers were prepared according to Phoebus software (Analis, Suarlee, Belgium) at a fixed ionic strength of 20 mM.

Permeation Experiments. Experimental conditions were slightly modified with respect to our original work[1] to better optimize the PAMPA assay for HTS applications: to have at least an unionized fraction (f_{ui}) > 0.8 for tested compounds, only three buffer solutions were used for acids, bases, and ionizable compounds at, respectively, pH = 2 for strong acids, pH = 6 for weak acids, weak bases, and unionizable compounds, and pH = 12 for strong bases.

The effective permeability coefficients P_e (cm/s) were calculated using the published equation below[24]

$$P_e = -\frac{2.303V_D}{A(t-\tau_{LAG})}\left(\frac{V_A}{V_A+V_D}\right)\times \log\left[1-\left(\frac{V_A+V_D}{V_D(1-R)}\right)\frac{C_A(t)}{C_D(0)}\right] \quad (5)$$

where A is the filter area (0.3 cm^2) multiplied by a nominal porosity of 70% according to the manufacturer, t is incubation time (s), τ_{LAG} is the steady-state time (s), that is, the time needed for the permeant's concentration gradient to become stabilized, V_A and V_D are respectively the volumes in the acceptor and the donor wells (0.28 cm^3), $C_A(t)$ is the concentration of the compound (mol cm^{-3}) in the acceptor well at time t, and $C_D(0)$ is the concentration of the compound (mol cm^{-3}) in the donor well at time 0. R is the retention factor defined as the mole fraction that is lost in the membrane and in the microplates (i.e., filters and plate materials)

$$R = 1 - \frac{C_D(t)}{C_D(0)} - \frac{V_A}{V_D}\times\frac{C_A(t)}{C_D(0)} \quad (6)$$

where $C_A(t)/C_D(0)$ represents the amount of compound that reached the acceptor compartment after the incubation time t (for $V_A = V_D$). Steady-state times (τ_{LAG}) to saturate the membranes in PAMPA are short relative to the total permeation time (~20 min with unstirred plates)[25] and for this reason they were considered negligible in this study.

Computational Procedure. The 3D structure of selected compounds was generated using Corina computer program as implemented in TSAR 3.3 (Oxford Molecular Ltd., Oxford, U.K.) and energy-optimized in vacuo ($\epsilon = 1$) with the MMFF94s force field available in Sybyl7.2 (Tripos, Inc., U.S.A.). Molecules were built in their neutral form, and salts were removed.

The MIFs were calculated using the MLP_{ho}, the acceptor and donor MHBPs, and the GRID "DRY" and "H_2O" fields.

The molecular lipophilicity potential (MLP) is a 3D representation of the lipophilicity encoded by all fragments in the molecule. A log P_{oct} value is attributed to each fragment of a molecule, and then the overall lipophilic potential is calculated at any given point in space around the molecule.[15] Positive MLP values describe hydrophobic parts of the molecule, whereas negative MLP values represent hydrophilic interactions. Solvatochromic analysis of the octanol−water log P for nonelectrolytes showed that wet octanol has a different H-bond donor capacity than water, while its H-bond acidity is similar to that of water.[18,19] Thus, the hydrophilic interactions described by the octanol−water partition coefficient do not fully represent the entire capacity of solutes to perform polar interactions. Therefore, only the MLP_{ho} was retained and the MHBPs were to describe the polar interactions of compounds. Indeed, MHBPs provide a description of 3D H-bonding properties of compounds and consist in a H-bonding donor potential (MHB-P_{don}) and a H-bonding acceptor potential.[16]

The GRID force field is widely used for determining energetically favorable binding sites on compounds of known structure,[17] and the interaction energies are computed between different probes and the target molecules. Because polar interactions were already described by MHBP, the GRID MIF generated by the interaction with a H_2O probe was only used to generate the global molecular parameters such as molecular volume (V), surface (S), globularity (G), and rugosity (R). However, it has been previously demonstrated that the interactions described by the DRY probe well encode for dipolarity/polarizability interactions (π^*).[26] As a consequence, the information contained in the interaction field described by GRID-DRY was merged with MLP and MHBP fields to build the 3D solvatochromic-type model. The Volsurf approach was then used to calculate molecular descriptors from 3D molecular interactions fields.[2]

The selected Volsurf descriptors calculated from the molecular interaction fields described above are summarized in Table 2.

Statistical Analysis. PLS analyses were performed with SIMCA-P11 (Umetrics AB, Umea, Sweden). PLS is a chemometric tool for extracting and rationalizing the information from any multivariate description of a system condensing the overall information

Table 2. Molecular Fields and Related Molecular Descriptors Calculated by VolSurf Program Used in the Study

molecular field	code	description
$GRID_{H_2O}$	V	molecular volume
$GRID_{H_2O}$	S	molecular surface
$GRID_{H_2O}$	R	ratio volume/surface
$GRID_{H_2O}$	G	molecular globularity
$GRID_{DRY}$	V-DRY	volumes of dipolarity/polarizability regions[a]
$GRID_{DRY}$	I-DRY	dipolarity/polarizability integy moments[a]
MLP_{ho}	V-MLP_{ho}	volumes of hydrophobic regions[a]
MLP_{ho}	I-MLP	hydrophobic integy moments[a]
$MHBP_{ac}$	V-$MHBP_{ac}$	volumes of H-bond acceptor regions[a]
$MHBP_{ac}$	I-$MHBP_{ac}$	H-bond acceptor integy moments[a]
$MHBP_{do}$	V-$MHBP_{do}$	volumes of H-bond donor regions[a]
$MHBP_{do}$	I-$MHBP_{do}$	H-bond donor integy moments[a]

[a] Calculated at eight energy levels.

into two smaller matrices, namely the score plot and the loading plot. Score plots are used to reveal the presence of clusters of objects while loading plots are useful to discover the relation between the original variables and the LVs. The PLS searches the linear relationship between a matrix **X** (independent variable) and a matrix **Y** (dependent variables). In this work, the log P_e was used as dependent variable (*Y*) in the PLS model, while for the discriminant-analysis DA-PLS model three classes were considered as dependent variables (*Y*) according to experimental values of membrane retention and permeation (see Results and Discussion for classification of permeants) using the following binary digit representation: for class (I), 1;0;0; for class (II), 0;1;0; and finally for class (III), 0;0;1. The "leave-one-out" cross-validation procedure was used to evaluate the predictive ability of the PLS models. The method builds reduced models and uses them to predict the *Y*-variables of the excluded objects.

Acknowledgment. The authors thank Fond National Suisse de la Recherche Scientifique (FNRS) for financial support. They are also grateful to Professor Gabriele Cruciani for inspiration and fruitful discussions.

References

(1) Ottaviani, G.; Martel, S.; Carrupt, P. A. Parallel artificial membrane permeability assay: A new membrane for the fast prediction of passive human skin permeability. *J. Med. Chem.* **2006**, *49*, 3948−3954.

(2) Cruciani, G.; Crivori, P.; Carrupt, P. A.; Testa, B. Molecular fields in quantitative structure permeation relationships: The VolSurf approach. *J. Mol. Struct.: THEOCHEM* **2000**, *503*, 17−30.

(3) Potts, R. O.; Guy, R. H. Predicting skin permeability. *Pharm. Res.* **1992**, *9*, 663−669.

(4) Mitragotri, S. Modeling skin permeability to hydrophilic and hydrophobic solutes based on four permeation pathways. *J. Controlled Release* **2003**, *86*, 69−92.

(5) Peck, K. D.; Ghanem, A. H.; Higuchi, W. I. The effect of temperature upon the permeation of polar and ionic solutes through human epidermal membrane. *J. Pharm. Sci.* **1985**, *84*, 975−962.

(6) Sekkat, N.; Kalia, Y. N.; Guy, R. H. Porcine ear skin as a model for the assessment of transdermal drug delivery to premature neonates. *Pharm. Res.* **2004**, *21*, 1390−1397.

(7) Flynn, G. L. Physicochemical determinants of skin absorption. In *Principles of Route-to-Route Extrapolation for Risk Assessment*; Gerrity, T. R., Henry, C. J., Eds.; Elsevier: Amsterdam, 1990; pp 93−127.

(8) Moss, G. P.; Dearden, J. C.; Patel, H.; Cronin, M. T. D. Quantitative structure−permeability relationships (QSPRs) for percutaneous absorption. *Toxicol. in Vitro* **2002**, *16*, 299−317.

(9) Geinoz, S.; Guy, R. H.; Carrupt, P. A.; Testa, B. Quantitative structure−permeation relationships (QSPeRs) to predict skin permeation: A critical review. *Pharm. Res.* **2004**, *21*, 83−92.

(10) Cronin, M. T. D.; Dearden, J. C.; Gupta, R.; Moss, G. P. An investigation of the mechanism of flux across polymethylsiloxane membranes by use of quantitative structure−permeability relationships. *J. Pharm. Pharmacol.* **1998**, *50*, 143−152.

(11) Katritzky, A. R.; Dobchev, D. A.; Fara, D. C.; Hür, E.; Tämm, K.; Kurunczi, L.; Karelson, M.; Varnek, A.; Solov'ev, V. P. Skin permeation rate as a function of chemical structure. *J. Med. Chem.* **2006**, *49*, 3305−3314.

(12) Kamlet, M. J.; Abboud, J. L. M.; Abraham, M. H.; Taft, R. W. Linear solvation energy relationships. 23. A comprehensive collection of the solvatochromic parameters, π^*, α, and β, and some methods for simplifying the generalized solvatochromic equation. *J. Org. Chem.* **1983**, *48*, 2877−2887.

(13) Abraham, M. H.; Martins, F. Human skin permeation and partition: General linear free-energy relationship analyses. *J. Pharm. Sci.* **2004**, *93*, 1508−1523.

(14) Weber, H.; Steimer, U.; Mannhold, R.; Cruciani, G. Synthesis, in vitro skin permeation studies, and PLS-analysis of new naproxen derivatives. *Pharm. Res.* **2001**, *18*, 600−607.

(15) Gaillard, P.; Carrupt, P. A.; Testa, B.; Boudon, A. Molecular lipophilicity potential, a tool in 3D-QSAR. Method and applications. *J. Comput.-Aided Mol. Design* **1994**, *8*, 83−96.

(16) Rey, S.; Caron, G.; Ermondi, G.; Gaillard, P.; Pagliara, A.; Carrupt, P. A.; Testa, B. Development of molecular hydrogen bonding potentials (MHBPs) and their application to structure permeation relations. *J. Mol. Graphics Modell.* **2001**, *19*, 521−535.

(17) Goodford, P. J. A computational procedure for determining energetically favorable binding sites on biologically important macromolecules. *J. Med. Chem.* **1985**, *28*, 849−857.

(18) Kamlet, M. J.; Doherty, R. M.; Abraham, M. H.; Marcus, Y.; Taft, R. W. Linear solvation energy relationships. 46. An improved equation for correlation and prediction of octanol/water partition coefficients of organic nonelectrolytes (including strong hydrogen bond donor solutes). *J. Phys. Chem.* **1988**, *92*, 5244−5255.

(19) Steyaert, G.; Lisa, G.; Gaillard, P.; Boss, G.; Reymond, F.; Girault, H. H.; Carrupt, P. A.; Testa, B. Intermolecular forces expressed in 1,2-dichloroethane/water partition coefficient: a solvatochromic analysis. *J. Chem. Soc., Faraday Trans.* **1997**, *93*, 401−406.

(20) Potts, R. O.; Guy, R. H. A predictive algorithm for skin permeability: The effects of molecular size and hydrogen bond activity. *Pharm. Res.* **1995**, *12*, 1628−1633.

(21) Vickers, C. F. H. Existence of reservoir in the stratum corneum—experimental proof. *Arch. Dermatol.* **1963**, *88*, 20−33.

(22) Teichmann, A.; Jacobi, U.; Weigmann, H.-J.; Sterry, W.; Lademann, J. Reservoir function of the stratum corneum: development of an in vivo method to quantitatively determine the stratum corneum reservoir for topically applied substances. *Skin Pharmacol. Physiol.* **2004**, *18*, 75−80.

(23) Sosted, H.; Basketter, D. A.; Estrada, E.; Johansen, J. D.; Patlewicz, G. Y. Ranking of hair dye substances according to predicted sensitization potency: Quantitative structure−activity relationships. *Contact Dermatitis* **2004**, *51*, 241−254.

(24) Avdeef, A. *Absorption and Drug Development*; John Wiley & Sons: Hoboken, NJ, 2003.

(25) Avdeef, A.; Strafford, M.; Block, E.; Balogh, M. P.; Chambliss, W.; Khan, I. Drug absorption in vitro model: Filter-immobilized artificial membranes. Studies of the permeability properties of lactones in piper methysticum forst. *Eur. J. Pharm. Sci.* **2001**, *14*, 271−280.

(26) Bajot, F.; Geinoz, S.; Rey, S.; Cruciani, G.; Guy, R. H.; Carrupt, P. A. The Volsurf approach in structure−permeation relationships: Molecular interaction fields focused on specific intermolecular interactions. *J. Mol. Graphics Modell.* **2007**, submitted for publication.

(27) Vistoli, G.; Pedretti, A.; Villa, L.; Testa, B. The solute−solvent system: Solvent constraints on the conformational dynamics of acetylcholine. *J. Am. Chem. Soc.* **2002**, *124*, 7472−7480.

(28) Mitragotri, S.; Edwards, D. A.; Blankstein, D.; Langer, R. A mechanistic study of ultrasonically-enhanced transdermal drug delivery. *J. Pharm. Sci.* **1995**, *84*, 697−706.

(29) Johnson, M. E.; Blankschtein, D.; Langer, R. Permeation of steroids through human skin. *J. Pharm. Sci.* **1995**, *84*, 1144−1146.

(30) Johnson, M. E.; Blankstein, D.; Langer, R. Evaluation of solute permeation through the stratum corneum: Lateral bilayer diffusion as the primary transport mechanism. *J. Pharm. Sci.* **1997**, *86*, 1162−1172.

(31) Johnson, M. E.; Mitragotri, S.; Patel, A.; Blankschtein, D.; Langer, R. Synergistic effects of chemical enhancers and therapeutic ultrasound on transdermal drug delivery. *J. Pharm. Sci.* **1996**, *85*, 670−679.

(32) Hansch, C.; Leo, A. *Exploring QSAR. Fundamentals and Applications in Chemistry and Biology*, ACS Professional Reference Book; American Chemical Society: Washington, 1995; pp 1−557.

(33) Bronaugh, R. L.; Congdon, E. R. Percutaneous absorption of hair dyes: Correlation with partition coefficients. *J. Invest. Dermatol.* **1984**, *83*, 124−127.

JM0611105